

## Climate and Vegetation in the Middle East: Interannual Variability and Drought Feedbacks

BENJAMIN F. ZAITCHIK,\* JASON P. EVANS, ROLAND A. GEERKEN, AND RONALD B. SMITH

*Department of Geology and Geophysics, Yale University, New Haven, Connecticut*

(Manuscript received 23 May 2006, in final form 9 November 2006)

### ABSTRACT

The Euphrates Plain (EP) experiences large interannual variability in vegetation cover, especially in areas of marginal rain-fed agriculture. Vegetation in this region is primarily limited by available soil moisture, as determined by winter precipitation, spring precipitation, and air temperature. Satellite analyses indicate that the springtime normalized difference vegetation index (NDVI) is negatively correlated with surface albedo, and that interannual variability in albedo in the EP produces an estimated forcing on the radiation balance that peaks at  $16.0 \text{ W m}^{-2}$  in May.

Simulations with a regional climate model indicate that surface energy fluxes during a drought year (1999) differed substantially from those during a year with normal precipitation (2003). These differences were geographically specific, with the EP exhibiting increased albedo and decreased sensible heat flux while the neighboring Zagros Plateau region showed no albedo effect, a large increase in sensible heat flux, and an offsetting reduction in latent heat flux. In both the EP and the Zagros there was a potential for positive feedbacks on temperature and drought in late spring, though the most likely feedback mechanisms differed between the two regions: in the EP surface brightening leads to cooling and reduced turbulent heat flux, while in the Zagros region reduced latent heat flux leads to warming and a deepening of the planetary boundary layer.

### 1. Introduction

Semiarid regions are subject to regular seasonal dryness and large interannual variability in precipitation. This results in variable vegetation cover on annual and interannual time scales, as both natural ecosystems and nonirrigated crops rely on soil moisture derived from seasonal rains or springtime snowmelt (Baldocchi et al. 2004; Dall'Olmo and Karnieli 2002; Evans and Geerken 2004; Weiss et al. 2004). Opportunistic annual species green up rapidly in response to wetting of the soil surface, and their vigor is primarily related to recent rainfall events. Winter crops and perennial vegetation have access to deeper reserves of soil moisture. Growth of these vegetation types depends on the precipitation pattern over weeks and months, on evaporative de-

mand, and, for some regions, on temperature constraints.

Climate-induced variability in semiarid vegetation is a matter of both ecological interest and economic concern, as strong sensitivity to climate can result in rapid land use change (Vanacker et al. 2005) and vulnerability to human-induced degradation (Evans and Geerken 2004). Over longer time scales, relatively small shifts in background climate may have a substantial influence on the distribution of ecosystems and, perhaps, the viability of agricultural and pastoral systems (deMenocal 2001; Hole 1994; Weiss and Bradley 2001). Interest in the climate sensitivities of semiarid vegetation—particularly crops and rangelands—is evident in the large body of research devoted to characterizing the relationships between precipitation, soil type, land management, and vegetation growth in water-stressed regions (e.g., Archer et al. 1995; Kremer et al. 1996; Lane et al. 1998; LeHouerou 1996).

There is also a substantial literature concerned with vegetation feedbacks on climate in semiarid regions. In an effort to understand the role of land-atmosphere interactions during the extended Sahel drought of the early 1970s, Charney (1975) hypothesized a negative albedo-precipitation feedback in which dry conditions

---

\* Current affiliation: Hydrologic Sciences Branch, NASA Goddard Space Flight Center, Greenbelt, Maryland.

---

*Corresponding author address:* Benjamin F. Zaitchik, Hydrologic Sciences Branch, NASA Goddard Space Flight Center, Code 614.3, Greenbelt, MD 20771.  
E-mail: bzaitchik@hsb.gsfc.nasa.gov

lead to surface brightening, a decrease in available energy, and reduced convection. This, in turn, leads to vegetation die-back and increased albedo. Charney's hypothesis has informed numerous studies on albedo-precipitation feedbacks, including detailed field campaigns (Eltahir 1998; Small and Kurc 2003), satellite analyses (Brunsell 2006; Courel et al. 1984), and global-scale modeling exercises (Laval and Picon 1986; Sud and Fennessy 1982). This line of investigation has revealed important interactions between vegetation, albedo, and climate. The nature of these interactions depends on scale and regional context, and the forcing mechanisms are not always obvious.

In addition to albedo effects, vegetation is thought to influence the atmosphere through a number of structural and physiological mechanisms. Vegetation status has a significant impact on surface roughness, and the decrease in roughness associated with drought, land clearing, or overgrazing can lead to decreases in aerodynamic conductivity to surface heat fluxes, limiting energy transport to the atmosphere, and reducing convection (Sud and Smith 1985; Zheng et al. 2002). Vegetation also exerts direct control on latent heat flux from the surface. An active vegetation cover tends to increase latent heat flux, due to increased soil infiltration and subsequent transpiration of otherwise unavailable moisture. Increased latent heat flux both humidifies the planetary boundary layer (PBL) and increases moist static energy (MSE) of near-surface air, increasing the potential for precipitation (Eltahir 1998; Shukla and Mintz 1982; Sud and Fennessy 1984). Such coupling between surface conditions and atmospheric processes is thought to be particularly strong in semiarid regions (Koster et al. 2004).

This study takes advantage of recent interannual climatic variability to characterize the climatic sensitivities of vegetation in the Middle East and to investigate the potential for land-atmosphere feedbacks in the region. In the first half of this study (sections 2–4) time series data from the Advanced Very High Resolution Radiometer (AVHRR), Systeme pour l'Observation de la Terre (SPOT)-Vegetation, and Moderate Imaging Spectrometer (MODIS) satellite sensors are used to describe seasonal and interannual patterns in vegetation and albedo. Data sources and processing are detailed in section 2. In section 3 the phenology of major land cover types is described, interannual variability over the period 1981–2001 is quantified using AVHRR, and the primary climatic drivers of vegetation variability are identified. In section 4 satellite data are used to test the hypothesis that springtime vegetation growth has an impact on surface albedo and the surface energy balance in both spring and summer.

The second half of the study focuses on the years 1999 and 2003—a drought year and a nondrought year, respectively—for detailed analysis of land-atmosphere processes during drought, including a functional comparison of the lowlands of the Euphrates Plain (EP) and the uplands of the neighboring Zagros Plateau. This is accomplished by applying the PSU/NCAR MM5 regional climate model (Dudhia 1993; Grell et al. 1994) in full-year simulations for both 1999 and 2003, with satellite-derived datasets used to provide lower boundary information on vegetation cover and surface albedo. Section 5 provides details on the MM5 simulations. Results of the MM5 experiments are presented in section 6, and in section 7 the potential for feedbacks on cloud cover and precipitation are discussed. General conclusions are offered in section 8.

## 2. Data processing

### a. Satellite data

The AVHRR satellite, with its 20-yr data record (1981–2001) and reasonably high spatial resolution (8 km), provides an excellent tool for the analysis of regional vegetation. AVHRR 10-day composites of surface reflectance and maximum normalized differential vegetation index (NDVI) were downloaded from the NASA Distributed Active Archive Center (DAAC). Next, following a method described by Los (1993), time series AVHRR data were calibrated against three fairly time-invariant desert targets located in the Saudi Arabian desert. The method removes effects of sensor degradation and corrects for calibration differences between different sensor systems. Where indicated, these corrected 10-day images were averaged to provide mean monthly values.

Broadband shortwave albedo ( $\alpha_{\text{AVHRR}}$ ) was calculated from AVHRR reflectance data ( $r_1, r_2$ ) using the empirical relationship of Liang et al. (2002):

$$\alpha_{\text{AVHRR}} = -0.3376r_1^2 - 0.2707r_2^2 + 0.7074r_1r_2 + 0.2915r_1 + 0.5256r_2 + 0.0035,$$

where  $r_1$  is red reflectance and  $r_2$  is reflectance in the near-infrared. This nonlinear formula performed quite well in initial validation (Liang et al. 2002). In the present study, reliability of the estimate was confirmed by comparison with the sophisticated albedo estimates provided by MODIS on board the *Terra* satellite. During the 19 months of sensor overlap, AVHRR yielded albedo estimates for the study area that had similar variability to those of the MODIS Bidirectional Reflectance Distribution Function (BRDF) albedo product (mod43B3) (correlation for average EP albedo  $r =$

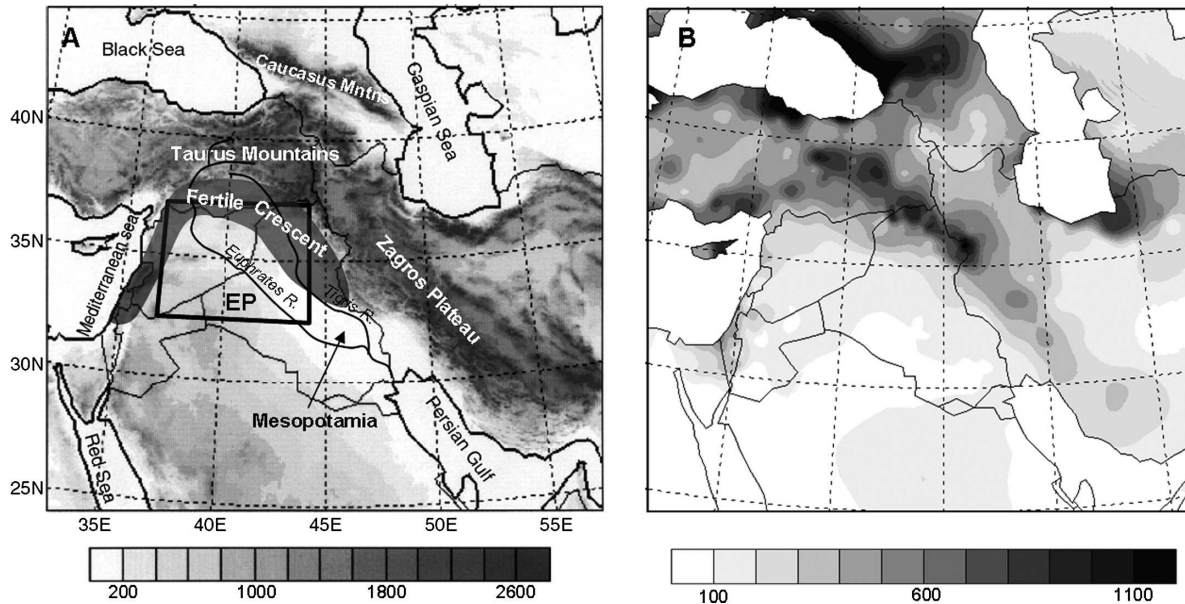


FIG. 1. The Middle East: (a) Major geographic features and topography (m); (b) mean annual precipitation from FAO reporting weather stations (1940–1973) interpolated using Cressman distance weighting (mm).

0.88). AVHRR-derived albedo was slightly, but consistently, lower than MODIS values by an average of 0.07 for the domain of interest. This offset would not be expected to affect the statistical analyses applied in this study.

For MM5 experiments, both albedo and green vegetation fraction were derived from 10-day composite images from the SPOT-Vegetation sensor. SPOT-Vegetation provides high quality, corrected surface reflectance data (Maisongrande et al. 2004), and the sensor was active in both 1999 and 2003, the two years of analysis in this study. Green vegetation fraction ( $f_g$ ) was calculated from SPOT NDVI using the linear vegetation index to percent cover conversion of Gutman and Ignatov (1998):

$$f_g = \frac{(\text{NDVI} - \text{NDVI}_0)}{(\text{NDVI}_\infty - \text{NDVI}_0)}$$

Minimum and maximum NDVI ( $\text{NDVI}_0$  and  $\text{NDVI}_\infty$ ) values were set to the minimum and maximum 10-day values for the study region over the available time series of SPOT-Vegetation data (1999–2005). Broadband albedo ( $\alpha_{\text{SPOT}}$ ) was calculated using the Liang et al. (2002) empirical reflectance-to-albedo relationship:

$$\alpha_{\text{SPOT}} = 0.3512r_1 + 0.1629r_2 + 0.3415r_3 + 0.1651r_4,$$

where  $r_{1-4}$  are reflectance in the blue, green, red, and near-infrared bands. SPOT-derived estimates of albedo were confirmed to be statistically similar to the MODIS BRDF albedo product over areas of comparison.

Information on land cover type is used only qualitatively in this study. Where possible, land use identification was accomplished by field visit. For other areas land cover type was determined using a satellite-derived Fourier filtered cycle similarity (FFCS) technique detailed in previous papers (Evans and Geerken 2006; Geerken et al. 2005b).

#### b. Climate data

Observational records of precipitation and temperature were extracted from the global summary of month observations collected at the Climate Prediction Center (CPC) of the National Centers for Environmental Prediction (NCEP). The study includes 824 stations, at least 600 of which reported in each month. Station data were interpolated using a Cressman analysis approach with variable radius of influence. A  $5^\circ\text{C km}^{-1}$  lapse rate correction was applied for interpolated temperatures, but no topographic correction was made to precipitation.

### 3. Vegetation types and variability in the Middle East

The Middle East is a predominantly semiarid region that contains a strong north to south precipitation gradient (Fig. 1). Humid regions of Turkey and Transcaucasia receive more than 1000 mm precipitation per year, while the deserts south of the Euphrates River receive  $100 \text{ mm yr}^{-1}$  or less. Interannual variability exceeds mean annual precipitation throughout the south-

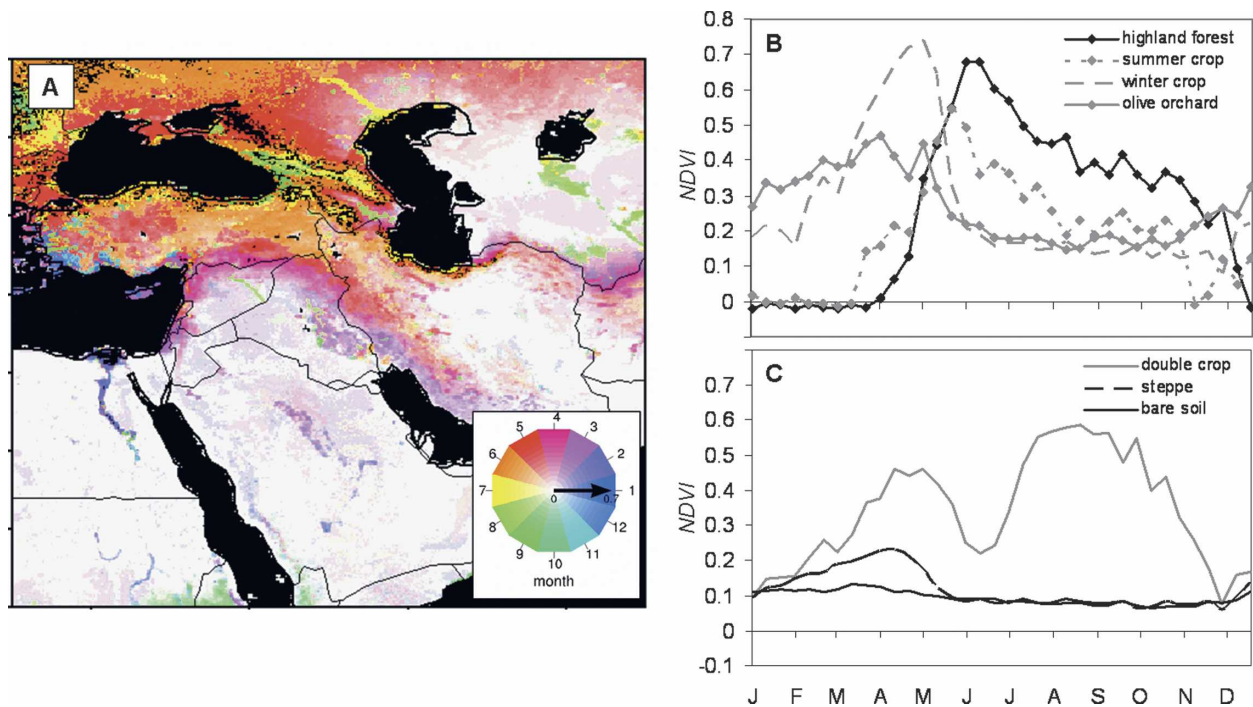


FIG. 2. Vegetation intensity in the Middle East. (a) Map of mean annual NDVI maximum, based on monthly averaged AVHRR data, 1981–2001. Color hue indicates the month of peak NDVI and color saturation indicates the magnitude of the NDVI peak. (b), (c) Phenology of representative pixels for major land cover types, based on SPOT 10-day NDVI composites for 2003.

ern portion of the region. This variability is of particular interest because it coincides with the southern limit of the historical Fertile Crescent agricultural zone and important rangelands of the Euphrates Plain. Present-day variability has a significant impact on crop yields and range productivity (Schmidt and Karnieli 2000; Weiss et al. 2001), and variability on longer time scales appears to be associated with the rise and fall of early civilizations (Weiss and Bradley 2001).

The north to south precipitation gradient is accompanied by an ecological gradient ranging from temperate forests and warm season agriculture in the north to winter crops, grasslands, and eventually shrublands and desert in the south. These land cover types differ in vegetation density and phenology (Fig. 2a). Forests in the highlands of Turkey are characterized by seasonally high NDVI, with vegetation intensity peaking in early summer and fading gradually in late summer and autumn (Fig. 2b). Rain-fed agriculture in the northern portion of the domain follows a similar pattern, returning negative NDVI values in the winter (indicative of snow cover), a rapid green-up in late spring, and relatively high NDVI throughout the long summer growing season. Agricultural phenologies in the Fertile Crescent are quite different. Here agriculture is limited by summertime dryness rather than wintertime frost, and the

NDVI of rain-fed crops peaks in late spring (Fig. 2b). Harvest of field crops in this region takes place in May and June. Orchard crops such as olive also have their phenologic peak in springtime, but the active growth period is both longer and more moderate (Fig. 2b). Along the river valleys and in regions of intense canal or groundwater irrigation a third field crop phenology is found, indicative of double-cropping practices (Fig. 2c). In these situations the winter crop may receive supplementary irrigation and the summer crop is entirely dependent on irrigation water. It should be noted that in AVHRR-based analysis many agricultural fields are contained within a single pixel, so a “double crop” phenology actually represents a composite of winter cropping, summer cropping, and some fields with active double cropping. Outside of irrigated areas, land cover south of the Fertile Crescent, east of the Caspian Sea, and in much of Iran is limited to sparse grasslands and shrubs. These lands are utilized seasonally for grazing, but they have extremely limited vegetation cover for much of the year. Phenologically, grasses and shrubs both green up in response to winter rains, peaking in March or April (Fig. 2c). Senescence comes rapidly in late spring, though this pattern varies with grazing pressure and the density of shrub cover, as shrubs have access to deeper moisture reserves and can stay green

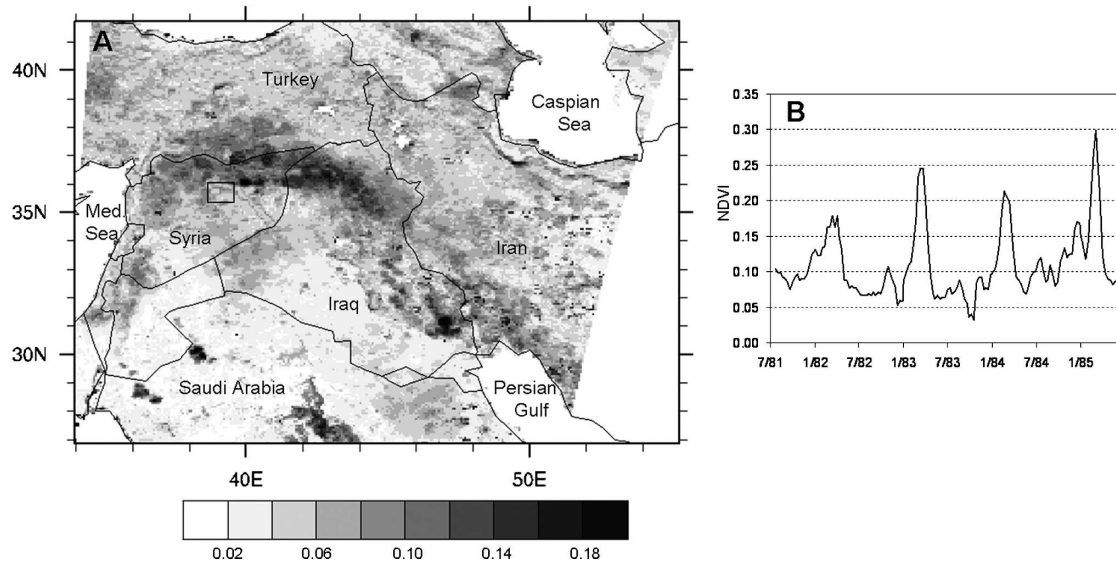


FIG. 3. NDVI variability, as captured by AVHRR monthly composites. (a) Map of the standard deviation in annual maximum NDVI value, 1982–2001. Box indicates the location of the Aleppo Steppe field experiment. (b) Subset of the AVHRR NDVI time series for a pixel within the Aleppo Steppe, giving an impression of typical annual and interannual variability at a rangeland location.

well into the dry season (Geerken et al. 2005b). Finally, much of the region is essentially barren, with no distinct NDVI phenology (Fig. 2c).

For the Tigris–Euphrates watershed, interannual variability in vegetation is greatest along the southern margin of the Fertile Crescent, an area which includes both rain-fed agriculture and semiarid rangelands (Fig. 3). In wet years this area is lush with grain crops and forage material, but in a drought year both crops and range vegetation can fail entirely. In addition to this swath of climate-driven variability, Fig. 3a shows hot spots of anthropogenic effects. These include the marshes of Mesopotamia, which experienced significant human modification over the study period (Nielsen and Adriansen 2005).

The nature of climate-driven variability can be explored by analyzing AVHRR data in conjunction with meteorological data. For each pixel in the study region, independent linear correlations were calculated between the annual maximum NDVI in AVHRR data ( $n = 20$  yr) and six variables that describe weather conditions in each hydrologic year: total precipitation in early winter (November–December), late winter (January–February), and spring (March–April), as well as average air temperature for the same three periods (data are described in section 2). Figure 4 maps the results of this analysis for all pixels with reasonably substantial vegetation coverage (mean annual  $\text{NDVI}_{\text{max}} > 0.12$ ) and significant climate sensitivity (linear correlation between  $\text{NDVI}_{\text{max}}$  and at least one

of the six climate variables significant at  $\alpha = 0.1$ ). Colors on the map indicate the climate variable for which the coefficient of linear correlation was largest for a given pixel. In highland regions of northern Iran, for example, we find that variability in NDVI correlates most strongly with wintertime temperatures (Fig. 4, area A): low wintertime temperatures in this area are associated with strong vegetation growth in spring. The negative correlation between wintertime temperature and  $\text{NDVI}_{\text{max}}$  can be attributed to the importance of subzero temperatures for the development of a winter snowpack, which is the primary source of springtime soil moisture.

Moving downslope and southward along the precipitation gradient, vegetation growth in the Fertile Crescent and rangelands of the EP correlates more strongly with precipitation than with temperature (Fig. 4, area B). The mediating factor is, again, soil moisture, but in this area snow is not a significant factor in the water balance of nonirrigated lands. Instead, soil moisture is replenished by winter and spring rains. In areas where soil moisture storage is sufficient, deep-rooted woody plants or winter crops are able to access moisture that infiltrated during winter rain events well into the spring, leading to a strong correlation between January–February precipitation and  $\text{NDVI}_{\text{max}}$ . In areas with shallow soils, or those dominated by opportunistic annual grass ecosystems,  $\text{NDVI}_{\text{max}}$  correlates most strongly with March–April precipitation, the period coinciding with the annual vegetation maximum.

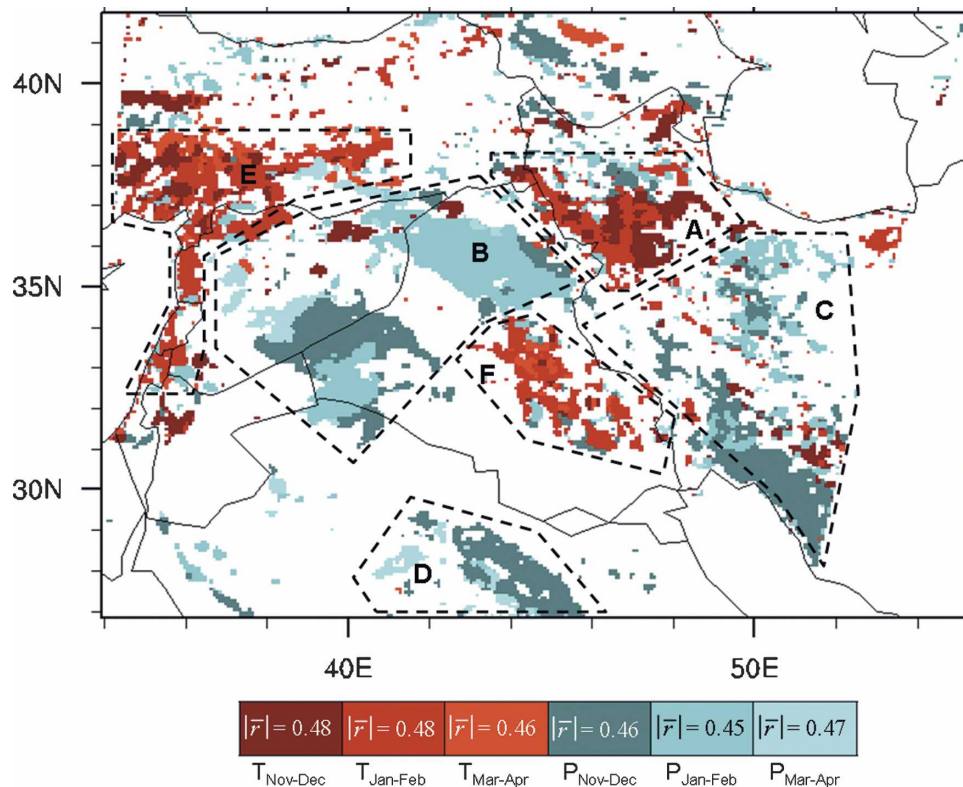


FIG. 4. Linear correlation between annual maximum NDVI and variables of winter/spring climate. Climate parameters are average air temperature and accumulated precipitation for Nov–Dec, Jan–Feb, and Mar–Apr in the hydrologic year of the NDVI maximum. Colors indicate the climate variable of greatest correlation for all pixels with mean annual  $\text{NDVI}_{\text{max}} > 0.12$  and linear correlation is significant at  $\alpha = 0.1$ . Mean correlation coefficient for each class is indicated on the label bar. Dashed lines indicate regions of coherent correlation type discussed in the text. Climate data are interpolated from the CPC weather station network; NDVI is derived from AVHRR, 1981–2001.

Sensitivity to precipitation is also dominant in the southern Zagros Plateau (area C), where vegetation includes hillslope grasses and several large agricultural areas. Somewhat surprisingly, a portion of arid north-central Saudi Arabia also exhibits sensitivity to precipitation (area D). The most striking vegetation features in this area are large cropped fields that are supported almost exclusively by groundwater irrigation (FAO 1997). The area also includes several large wadis, however, and it is possible that the detected climate sensitivity results from the response of natural vegetation to rare wadi floods.

Finally, some areas show a significant positive correlation between air temperature and  $\text{NDVI}_{\text{max}}$ . These areas fall in two regions. First, along the Mediterranean coast and in south-central Turkey (area E) the correlation with temperature reflects the fact that cold winters limit the growth of winter crops and orchards, which normally peak early in the year (Fig. 2a). The area is humid relative to the interior of the Middle East (mean

annual precipitation of  $350\text{--}700\text{ mm yr}^{-1}$ ), so the correlation between vegetation and precipitation is less important. The second region of positive temperature sensitivity is Mesopotamia (area F). Land use in this region includes vast areas of irrigated agriculture, so vegetation growth is decoupled from local precipitation. Instead, warm winters allow for healthy growth of the cold season crop and a higher peak NDVI.

#### 4. Albedo and the surface energy balance

Vegetation is known to impact surface albedo in several ways. The most direct effect is that photosynthetically active vegetation is dark in the visible range of the electromagnetic spectrum, where incoming solar radiation is greatest. This means that live plant material reflects less solar radiation than most semiarid soils (Charney et al. 1977). Senescent or dormant vegetation also influences surface albedo. Dry herbaceous material is relatively bright, so the presence of leaf litter over a wet or dark soil can cause an increase in albedo.

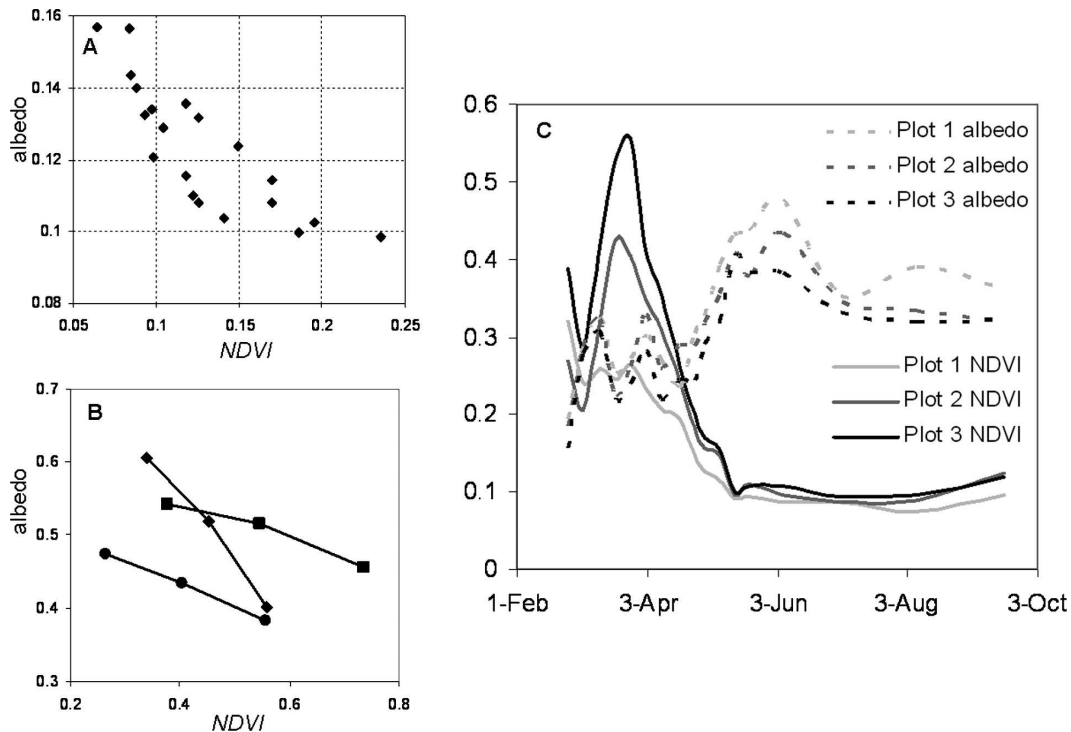


FIG. 5. NDVI and albedo. (a) Scatterplot of June albedo against March NDVI for 20 years of AVHRR data, averaged for all pixels in the MEP. (b), (c) Relationship between NDVI and broadband albedo for steppe vegetation (shrub and grass), measured using a portable spectrometer in the Aleppo Steppe (Syria; Fig. 3) in 2001. (b) Annual maximum albedo plotted against annual maximum NDVI for three subplots at three different field sites in the steppe. Lines connect the three subplots measured within each field site. Subplots were selected to capture a representative range of vegetation site cover. (c) Weekly NDVI and albedo derived from spectrometer readings for the three subplots at one study site [the solid diamond ( $\blacklozenge$ ) site in (b)].

Woody material, on the other hand, tends to be darker than dry leaves. Dormant trees and shrubs also cast shadow, reducing the total solar radiation incident on the soil surface. If the background soil is brighter than the woody material itself, then this effect will lead to a decrease in effective albedo and an increase in absorbed radiation.

Over 20 years of AVHRR data, there was a consistent negative correlation between spring NDVI in the EP and albedo in both spring and summer; that is, strong springtime vegetation made for a darker surface throughout the summer months. This correlation is strongest in the rangelands and is observed as a non-significant tendency for the EP on the whole (EP average statistics:  $r = -0.44$ ,  $p = 0.13$ ; Fig. 5a). There are three reasons for this correlation in the rangelands. First, at the resolution of an AVHRR pixel, the NDVI signal can be dominated by wadis and depressions that remain green throughout the summer in years with plentiful runoff. These concentrated areas of dark vegetation reduce the reflectance values recorded for the entire pixel. Second, certain succulent shrubs that are

unpalatable to livestock can retain green vegetation well into the dry season (Geerken and Iaiwi 2004), and these shrubs are most green in years with good precipitation. Third, summer albedo is negatively correlated with summer NDVI due to the structural effects of woody vegetation described above. Thus, the albedo effect can persist even after all green vegetation has senesced. This third phenomenon was confirmed in a field experiment in the Aleppo Steppe: regular measurements with a portable spectrometer indicated that high spring NDVI was associated with low summer albedo across a variety of rangeland environments, even after differences in NDVI had dropped to near zero (Figs. 5b and 5c; Geerken et al. 2005a).

To carry the analysis a step further, it is possible to calculate the influence of interannual variability in surface albedo on the absorption of shortwave radiation, using AVHRR estimates of albedo and the 40-yr NCEP-NCAR Reanalysis Project (NNRP; Kalnay et al. 1996) estimates of surface-incident shortwave radiation. According to this calculation, the interannual standard deviation in surface albedo is associated with a forcing on

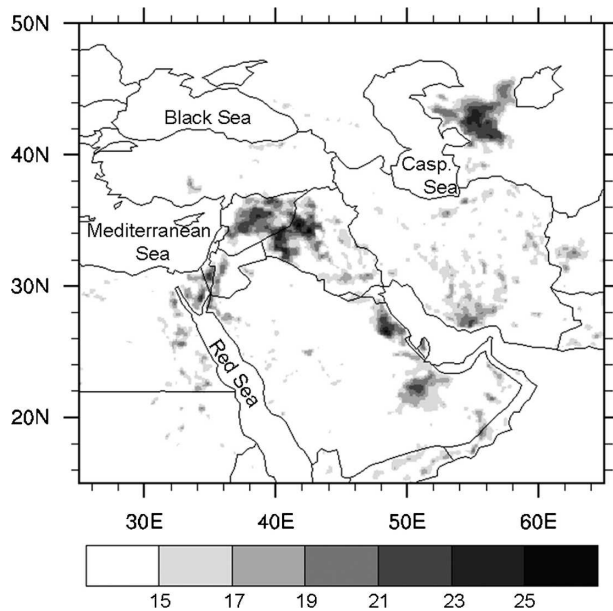


FIG. 6. Interannual standard deviation in absorbed short-wave radiation ( $\text{W m}^{-2}$ ), averaged over the month of May. Values are calculated using NNRP incoming shortwave radiation and AVHRR-derived surface albedo, 1981–2001. Note that maxima exist in the semiarid pasture lands of the EP, Ustyurt Plateau (east of the Caspian Sea), and Arabian Peninsula. Shading indicates areas where the interannual standard deviation exceeds  $15 \text{ W m}^{-2}$ .

the surface radiation balance that exceeds  $10.0 \text{ W m}^{-2}$  in every month from March through August, averaged monthly for the EP. This forcing peaks at  $16.0 \text{ W m}^{-2}$  for the month of May (Fig. 6). The effect is strongest in areas with large interannual variability in albedo and, it must be emphasized, is an average that includes much higher daytime values.

To put this forcing in context, the radiative forcing associated with a doubling of atmospheric  $\text{CO}_2$  is on the order of  $3.7 \text{ W m}^{-2}$  (Myhre et al. 1998). In a regional climate modeling study, Schär et al. (2004) found that a  $17.1 \text{ W m}^{-2}$  increase in net surface radiation was sufficient to produce feedbacks on precipitation in sensitive regions. Clearly, interannual variability in albedo in the EP has the potential to have a considerable impact on local temperatures and, potentially, hydrometeorology on the regional scale. These effects are investigated in greater detail in sections 5 and 6.

## 5. MM5 simulations

### a. 1999 and 2003

Between 1998 and 2001 much of the Middle East experienced an extended drought (DePauw 2004). The driest year was 1999, when spatially averaged annual precipitation in the EP was only 91.5 mm [CPC Merged

Analysis of Precipitation (CMAP); Xie and Arkin (1996)]. The rainy season of 2003 represented a return to normal hydrologic conditions. The year was not uniformly wet throughout the Middle East, but large portions of the region received precipitation that was at or above the long-term average. The EP received 163.2 mm of precipitation, and precipitation was greater in 2003 than in 1999 for every month of the rainy season (Fig. 7a). NDVI was correspondingly higher across the EP and most of the Zagros Plateau.

### b. MM5 experiments

The application of MM5 and the NCEP–Oregon State University–U.S. Air Force–Hydrologic Research Laboratory (NOAH) land surface model (LSM) to this region has been described elsewhere (Evans and Smith 2005; Zaitchik et al. 2005). The standard, limited-area, nonhydrostatic PSU–NCAR MM5 is used (Dudhia 1993; Grell et al. 1994), implemented with the Reisner mixed-phase explicit moisture scheme (Reisner et al. 1998), the Rapid Radiative Transfer Model (RRTM) radiation scheme (Mlawer et al. 1997), Grell’s cumulus scheme (Grell et al. 1994), and the Medium-Range Forecast (MRF) model’s planetary boundary layer scheme (Hong and Pan 1996). The MRF scheme is a first-order, nonlocal scheme optimized to represent large-eddy turbulence in a well-mixed PBL. In a comparison study of MM5 PBL schemes performed for the southwestern United States—a region that contains both intense deserts and significant topography, much like the Middle East—it was found that first-order closure schemes, including MRF, produced the highest accuracy predictions of PBL depth, CAPE, and vertical profiles of temperature and mixing ratio (Bright and Mullen 2002).

The NOAH LSM is used in its coupled form. Noah is a direct descendent of the Oregon State University (OSU) LSM (Mahrt and Pan 1984; Mahrt and Ek 1984; Pan and Mahrt 1987), a sophisticated land surface model that has been extensively validated in both coupled and uncoupled studies (Chen and Mitchell 1999; Chen and Dudhia 2001). The NOAH LSM simulates soil moisture, soil temperature, skin temperature, snowpack depth and water equivalent, canopy water content, and the energy flux and water flux terms of the surface energy balance and surface water balance. In its MM5-coupled form NOAH has a diurnally dependent Penman potential evaporation (Mahrt and Ek 1984), a four-layer soil model (Mahrt and Pan 1984), a primitive canopy model (Pan and Mahrt 1987), modestly complex canopy resistance (Jacquemin and Noilhan 1990), and a surface runoff scheme (Schaake et al. 1996). Additionally, an irrigation scheme was implemented that

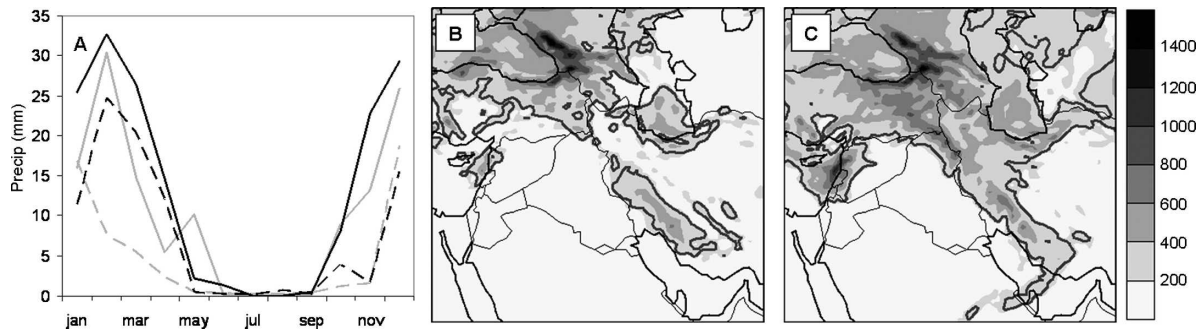


FIG. 7. (A) CMAP (black lines) and MM5-simulated precipitation (gray lines), averaged monthly for the EP in 1999 (dashed lines) and 2003 (solid lines). MM5-predicted total precipitation for (b) 1999 and (c) 2003, based on control simulations. The heavy contour in (b) and (c) corresponds to  $250 \text{ mm yr}^{-1}$ , the theoretical limit for rain-fed agriculture in the region.

realistically approximates flood irrigation practices of the region (Zaitchik et al. 2005). The use of a coupled land–atmosphere modeling system was deemed necessary in this study because of the tightly coupled nature of interactions between surface fluxes, PBL dynamics, and clouds (Betts 2004). For this reason, the results of sensitivity studies performed with uncoupled LSMs can be misleading in the analysis of physical process (Zhang et al. 2001).

For all simulations the model was implemented at 27-km horizontal resolution and with 23 levels in the vertical. Initial conditions and lateral boundary conditions were drawn from the NRP (Kalnay et al. 1996). To capture the effects of interannual vegetation variability it was necessary to integrate satellite-derived datasets for surface albedo and vegetation fraction. As described in an earlier study (Zaitchik et al. 2005), operational datasets currently available for MM5 provide only climatological estimates for these properties.

Four 14-month MM5 simulations were performed. First, control simulations were run for 1 November 1998–31 December 1999 and 1 November 2002–31 December 2003. In each case the first two months were treated as spinup and results were recorded for the calendar year. For these simulations surface albedo and vegetation fraction were drawn from SPOT-Vegetation data for the corresponding time period (see Section 2), and they are hereafter referred to as  $1999_{V1999}$  and  $2003_{V2003}$ , where the subscript indicates the year of satellite data. It was necessary to prescribe albedo as well as vegetation fraction because vegetation fields do not inform the predicted surface albedo field in MM5–NOAH. Next, “vegetation reversal” simulations were performed for the same time periods in which SPOT albedo and vegetation fraction from the nondrought year (2003) were input to MM5 simulations for the drought year (1999) and vice versa. These simulations are hereafter referred to as  $1999_{V2003}$  and  $2003_{V1999}$ .

It is important to note that the vegetation reversal experiments include the reversal of vegetation fraction, which is explicitly a property of vegetation, and surface albedo, which may be influenced by a number of factors, notably soil moisture. It is the authors’ contention that variability in the albedo field is associated primarily with vegetation rather than soil moisture. The SPOT images used to derive the surface albedo were acquired in late morning under clear-sky conditions. For the highly evaporative conditions that predominate in the Middle East in late spring (the season of primary interest), the soil surface is generally dry by this time of day, minimizing the impact that residual soil moisture can have on remotely sensed surface albedo. For this reason it can be stated that vegetation reversal experiments have the potential to capture vegetation–climate feedbacks, but not soil moisture–climate feedbacks, both of which may operate during a drought. If our assumption is incorrect and albedo is under strong control of soil moisture, then soil moisture–climate feedbacks related to albedo are included in the analysis, while those related to the evaporation of soil water are not. In either case, the inclusion of albedo in the vegetation reversal experiment leads to results that are different from vegetation reversal studies that have not included albedo (e.g., Matsui et al. 2005).

### c. Statistical analysis

For results presented as spatial averages, the significance of differences between simulations was tested using a Student’s *t* test. To minimize the influence of spatial autocorrelation, only a subset of grid points was included in our statistical analysis, such that there was a minimum distance of 108 km (four grid cells) separating any two points included in the analysis. This resulted in  $n = 18$  points for both the EP and northern Zagros Plateau (NZ) subregions. The analysis cannot assess

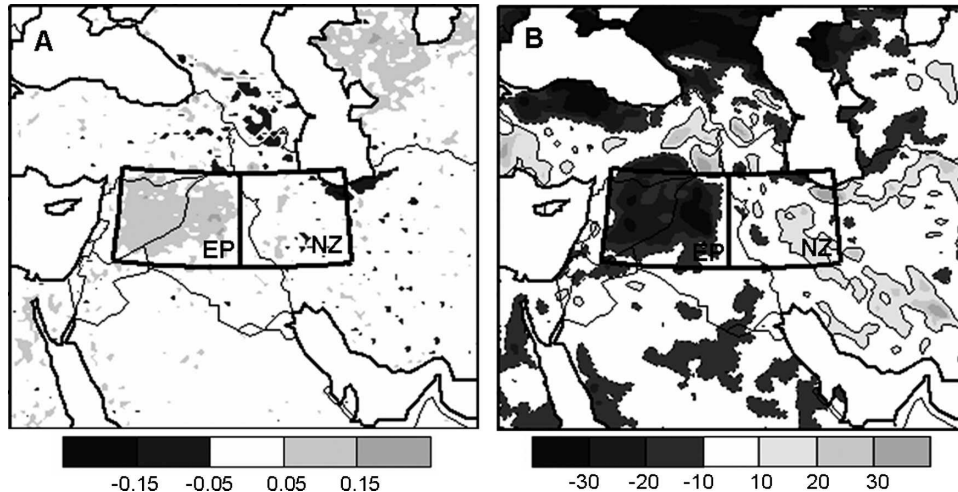


FIG. 8. Average difference for the month of May, 1999–2003, in (a) surface albedo and (b) net surface radiation, according to MM5 simulations. Boxes EP and NZ indicate the Euphrates Plain and Northern Zagros subregions described in the text and in Tables 1 and 2. In (b), regions of positive difference are outlined by solid lines and regions of negative difference are outlined by dashed lines.

the significance of results relative to the uncertainty in atmospheric drivers, but it does establish the significance of the differences relative to regional variability in the MM5 simulations. All reported  $t$  tests are for monthly averaged MM5 output.

## 6. Results of MM5 simulations

As expected, the MM5 returned drier conditions in  $1999_{V1999}$  than in  $2003_{V2003}$ . Precipitation results were reasonably similar to the CMAP integrated observations (Fig. 7a), and precipitation was, in general, greater in 2003 across the Euphrates Plain and the Zagros Plateau (Figs. 7b and 7c). For the EP the difference in precipitation was present only in the rainy and transitional seasons, as June–September was almost completely dry in both years. Strong wintertime precipitation in 2003 led to an extensive snowpack that persisted through April in highland areas of Turkey and Iran.

For both years, snow retreated from most of the Taurus and Zagros regions by May. May is an interesting month for analysis because it lies in the transition between the rainy season of winter and spring and the persistent aridity of summer. The intrusion of large storm systems into the region is reduced relative to November–April, allowing for greater local influence on the atmosphere, but significant precipitation is still observed in most years, indicating a potential for moist convection. For these reasons, May is a period during which precipitation processes are expected to be sensitive to a land–atmosphere forcing involving persistent spring vegetation or soil moisture.

From the perspective of land–atmosphere interactions, it is important to note that the 1999 drought led to an increase in albedo only in the semiarid lowland areas of the EP and, in the northeast of the study region, the Caspian steppe. In the Zagros foothills and plateau—where soil moisture is greater, soils are darker, and vegetation is less sensitive to precipitation drought—there was no detectable difference in May surface albedo between 1999 and 2003 (Fig. 8a; Table 1). In August a small difference between 1999 and 2003 albedo in the northern Zagros did develop (+0.03, not shown), but this difference was at all times smaller than that in the EP, and it occurred at a time of year when precipitation is strongly inhibited by large-scale circulations (Rodwell and Hoskins 1996; Ziv et al. 2004), limiting the potential for local feedbacks. This spatial variability in albedo is important because of its implications for the surface radiation balance. If we consider the two neighboring subregions of the EP and the NZ, the MM5 simulations indicate that net radiation available at the surface ( $R_{\text{net}}$ ) was reduced in the EP ( $p < 0.0001$ ) but not in the NZ (Fig. 8b). In fact,  $R_{\text{net}}$  tended to be slightly greater in 1999 for the Zagros, due to clear-sky conditions and an increase in solar radiation incident on the ground surface, though this tendency was not significant ( $p = 0.359$ ). This contrast in  $R_{\text{net}}$  was associated with a contrast in ground temperature. In the EP the warm synoptic conditions of 1999 were offset by a decrease in local  $R_{\text{net}}$ , such that the average ground temperature in May was no higher in 1999 than in 2003 ( $t$  test for difference:  $p = 0.960$ ). In the NZ, in contrast, the increase in  $R_{\text{net}}$  in 1999 combined with a

TABLE 1. Surface fluxes and PBL properties for MM5 control simulations. Values are averages for the month of May for albedo ( $\alpha$ ); near-surface soil moisture ( $SM_{0-10\text{cm}}$ ); incoming and reflected solar radiation at the surface ( $S_{\downarrow}$ ,  $S_{\uparrow}$ ); surface-incoming and surface-emitted longwave radiation ( $L_{\downarrow}$ ,  $L_{\uparrow}$ ); net surface radiation ( $R_{\text{net}}$ ); ground temperature ( $T_{\text{ground}}$ ); sensible heat flux ( $H$ ); latent heat flux ( $\lambda E$ ); conductive heat flux to the subsurface ( $G$ ); depth and temperature of the planetary boundary layer ( $\text{Depth}_{\text{PBL}}$ ,  $T_{\text{PBL}}$ ); turbulent, radiative, and total surface heat fluxes ( $Q_t$ ,  $Q_R$ ,  $Q_{\text{Total}}$ ); local contribution to the moist static energy density of the PBL ( $\langle \text{MSE} \rangle_{\text{local}}$ ); and precipitation.

Variable	Unit	Euphrates Plain			Northern Zagros		
		1999	2003	1999–2003	1999	2003	1999–2003
$\alpha$	—	0.31	0.25	0.06	0.19	0.19	0.00
$SM_{0-10\text{cm}}$	$\text{m}^{-3} \text{m}^{-3}$	0.132	0.160	−0.028	0.148	0.215	−0.067
$S_{\downarrow}$	$\text{W m}^{-2}$	344.7	330.5	14.2	331.8	301.9	29.9
$S_{\uparrow}$	$\text{W m}^{-2}$	106.9	82.6	24.2	63.0	57.4	5.7
$L_{\downarrow}$	$\text{W m}^{-2}$	337.4	344.2	−6.8	306.4	311.3	−4.9
$L_{\uparrow}$	$\text{W m}^{-2}$	459.3	459.3	0.0	424.2	406.6	17.6
$R_{\text{net}}$	$\text{W m}^{-2}$	116.0	132.8	−16.8	151.0	149.3	1.7
$T_{\text{ground}}$	$^{\circ}\text{C}$	300.0	300.0	0.0	294.1	291.0	3.1
$H$	$\text{W m}^{-2}$	99.5	105.6	−6.1	114.3	81.9	32.4
$\lambda E$	$\text{W m}^{-2}$	6.6	16.2	−9.6	25.4	55.1	−29.7
$G$	$\text{W m}^{-2}$	6.4	7.4	−1.0	8.0	9.9	−1.9
$\beta$	—	15.08	6.52	8.56	4.50	1.49	3.01
$\text{Depth}_{\text{PBL}}$	m	1270	1397	−127	1477	1207	270
$Q_t$	$\text{W m}^{-2}$	106.1	121.8	−15.7	139.7	137.0	2.7
$T_{\text{PBL}}^*$	$^{\circ}\text{C}$	293.1	292.1	1.0	281.8	278.9	2.9
$Q_R$	$\text{W m}^{-2}$	−142.9	−137.2	−5.7	−103.0	−99.1	−3.9
$Q_{\text{total}}$	$\text{W m}^{-2}$	−36.8	−15.4	−21.4	36.7	37.9	−1.2
$\langle \text{MSE} \rangle_{\text{local}}$	$\text{W m}^{-3}$	−0.029	−0.011	−0.018	0.025	0.031	−0.007
Precip	mm	0.6	10.1	−9.5	4.6	20.3	−15.7

\*  $T_{\text{PBL}}$  is taken at a height near the top of the average PBL: 850 hPa for EP and 700 hPa for NZ.

substantial reduction in soil moisture to enhance large-scale advective warming, producing radiative ground temperatures that were  $3.1^{\circ}\text{C}$  warmer in May 1999 relative to May 2003 (Table 1;  $p = 0.003$ ). This MM5 result is consistent with NNRP estimates of the 2-m air temperature for the same period: according to the NNRP, May 1999 was only  $0.1^{\circ}\text{C}$  warmer than May 2003 for the EP, while it was  $1.3^{\circ}\text{C}$  warmer for the NZ.

The difference in drought impact on  $R_{\text{net}}$  in the EP versus the NZ also has an impact on turbulent heat flux via the surface energy balance:  $R_{\text{net}} = H + \lambda E + G$ , where  $H$  is net surface sensible heat flux,  $\lambda E$  is surface latent heat flux, and  $G$  is conductive heat flux from the surface to subsurface. The drought-related reduction in  $R_{\text{net}}$  in the EP for 1999 was associated with a decrease in  $H$  of  $6.1 \text{ W m}^{-2}$  relative to 2003 ( $p < 0.0001$ ), averaged over the month of May, while the clear-sky-associated increase in  $R_{\text{net}}$  for the NZ was associated with an increase in  $H$  of  $32.4 \text{ W m}^{-2}$  ( $p < 0.0001$ ). Latent heat flux ( $\lambda E$ ), meanwhile, was reduced in 1999 for both the EP (by  $9.6 \text{ W m}^{-2}$ ;  $p = 0.0007$ ) and the NZ (by  $29.7 \text{ W m}^{-2}$ ;  $p < 0.0001$ ) due to reduced soil moisture. The effect was considerably larger in the NZ area because soil moisture in the EP was quite low in May even in the relatively wet year of 2003.

### Vegetation reversal

Vegetation reversal experiments have the potential to clarify the relative importance of synoptic forcing and local vegetation properties during drought. The “reversals” of the surface properties performed in this experiment capture the effects of drought on albedo and latent heat flux. Surface roughness effects were not captured by these experiments, as roughness is not a predicted field in the MM5–NOAH simulations, and the parameter was left at land cover defaults for all simulations. Latent heat flux effects could arise as a result of greater access to soil moisture, which is a function of vegetation fraction in MM5–NOAH (Chen and Dudhia 2001), or as a secondary product of albedo since an increase in net radiation at the surface would be expected to increase the total turbulent energy transfer. In application, however, vegetation reversal had no significant effect on the May latent heat flux in the EP (Table 2;  $p = 0.960$ ). By this time of the year model soil moisture was depleted in the EP in both 1999 and 2003, leaving little possibility for vegetation to influence latent heat flux. What difference there was in  $\lambda E$  between 1999 and 2003 (Table 1) primarily arose from direct soil evaporation after rain events, and

TABLE 2. Impact of vegetation reversal on MM5 simulations. Values reported are differences that indicate the impact of drought vegetation ( $1999_{V1999}$ ,  $2003_{V1999}$ ) as opposed to healthy vegetation ( $1999_{V2003}$ ,  $2003_{V2003}$ ) in each simulation year. Symbols are defined in Table 1.

Variable	Unit	Euphrates Plain		Northern Zagros	
		$1999_{V1999}$ – $1999_{V2003}$	$2003_{V1999}$ – $2003_{V2003}$	$1999_{V1999}$ – $1999_{V2003}$	$2003_{V1999}$ – $2003_{V2003}$
$\alpha$	—	0.06	0.06	0.00	0.00
$SM_{0-10\text{cm}}$	$\text{m}^{-3} \text{m}^{-3}$	–0.002	–0.002	–0.004	–0.004
$S_{\downarrow}$	$\text{W m}^{-2}$	1.1	3.5	4.3	4.1
$S_{\uparrow}$	$\text{W m}^{-2}$	21.0	20.9	0.8	0.8
$L_{\downarrow}$	$\text{W m}^{-2}$	–2.9	–4.1	–2.8	–1.4
$L_{\uparrow}$	$\text{W m}^{-2}$	–6.2	–6.7	0.0	0.0
$R_{\text{net}}$	$\text{W m}^{-2}$	–16.6	–14.8	0.7	1.9
$T_{\text{ground}}$	$^{\circ}\text{C}$	–1.0	–1.1	0.0	0.0
$H$	$\text{W m}^{-2}$	–17.0	–15.7	5.3	2.5
$\lambda E$	$\text{W m}^{-2}$	–0.3	–0.3	–5.6	–0.6
$G$	$\text{W m}^{-2}$	–0.2	1.1	0.0	–0.3
Depth <sub>PBL</sub>	m	–165	–156	–5	4
$Q_t$	$\text{W m}^{-2}$	–17.3	–16.0	–0.3	1.9
$T_{\text{PBL}}^*$	$^{\circ}\text{C}$	–0.5	–0.5	–0.1	–0.1
$Q_R$	$\text{W m}^{-2}$	–0.8	–1.2	0.5	0.5
$Q_{\text{total}}$	$\text{W m}^{-2}$	–18.1	–17.2	0.2	2.4
$\langle \text{MSE} \rangle_{\text{local}}$	$\text{W m}^{-3}$	–0.016	–0.015	0.000	0.002
Precip	mm	0.0	–0.9	–0.4	–0.8

\*  $T_{\text{PBL}}$  is taken at a height near the top of the average PBL: 850 hPa for EP and 700 hPa for NZ.

this flux was not significantly affected by vegetation status.

In the NZ, modeled  $\lambda E$  for May was substantial in both 1999 and 2003. In May 2003, in fact, soil moisture was so great that actual evapotranspiration (AET) frequently approached the atmospherically limited rate of potential evapotranspiration (PET). Under such moist conditions, the access to deeper reserves of soil moisture afforded by healthy vegetation does not have a substantial impact on  $\lambda E$ . In 1999, when there was little precipitation in May, the soil surface dried out and  $\lambda E$  was reduced by more than 50% (Table 1). Under these drier conditions AET was well below PET due to moisture limitation. Vegetation access to subsurface soil moisture thus has the potential to influence the partitioning of surface energy. In 1999, the average MEP  $\lambda E$  was reduced by  $5.6 \text{ W m}^{-2}$  in the simulation with drought vegetation ( $1999_{V1999}$ ) relative to that with nondrought vegetation ( $1999_{V2003}$ ), though the difference was not statistically significant ( $p = 0.140$ ).

Vegetation reversal had a substantial impact on radiation fluxes in the EP for both 1999 and 2003 simulations. In both years, drought vegetation was associated with increased albedo and reduced  $R_{\text{net}}$  ( $p < 0.0001$ ). Reduced  $R_{\text{net}}$  led to lower ground temperature (significant for 2003,  $p_{2003} = 0.050$ ; nonsignificant for 1999,  $p_{1999} = 0.109$ ), reduced sensible heat flux ( $p < 0.0001$ ), and a shallower PBL ( $p < 0.0001$ ) (Figs. 9a–c). Drought vegetation also led to a reduction in total tur-

bulent heat flux from the surface ( $Q_t$ ; Table 2) and an elevated lifting condensation level (LCL; Fig. 9d), the implications of which will be discussed in the following section. In the NZ, where the 1999 drought did not affect the May surface albedo, the vegetation reversal experiment had no significant impact on radiation fluxes in either year ( $R_{\text{net}} p_{1999} = 0.140$ ,  $p_{2003} = 0.597$ ). Ground temperature, sensible heat flux, and the depth of the PBL were also unaffected ( $p > 0.2$  for all analyses). As in the interannual comparison, the vegetation reversal experiments did yield some effects on albedo and  $R_{\text{net}}$  for the NZ in July and August. These effects were small relative to those in the EP in May and, as mentioned above, they arise during a season when a land–atmosphere forcing on precipitation is unlikely to occur.

## 7. Feedbacks on cloudiness and precipitation

Two hypotheses for a drought feedback on precipitation are considered: a mechanism associated with reduced  $R_{\text{net}}$  (Eltahir 1998) and a mechanism involving deepening and drying of the planetary boundary layer (Betts and Ball 1998). These hypotheses have been reviewed and compared in detail by Small and Kurc (2003) and Zaitchik et al. (2006). Briefly, in the mechanism proposed by Eltahir (1998) a drought-related increase in albedo and decrease in soil moisture leads to a reduction in  $R_{\text{net}}$  and an associated reduction in total

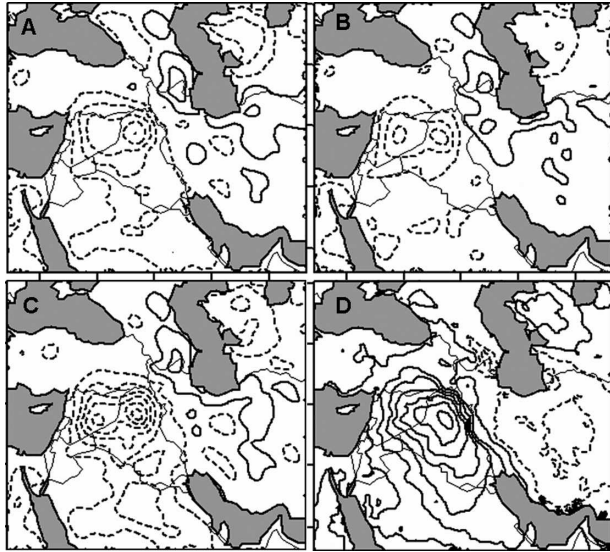


FIG. 9. Results of MM5 vegetation reversal experiment for 1999, expressed as the difference  $1999_{V1999} - 1999_{V2003}$ : (a) ground temperature ( $^{\circ}\text{C}$ ), (b) sensible heat flux ( $\text{W m}^{-2}$ ), (c) PBL depth (m), and (d) lifting condensation level (m). Contour intervals are 0.4 (a), 10.0 (b), (d), and 50.0 (c), centered on zero, with negative contours dashed.

turbulent heat flux from the surface ( $Q_t = H + \lambda E$ ). This means that the local land surface contributes less to the moist static energy (MSE) of the PBL during drought than it would under normal conditions. The density of MSE in the PBL is directly associated with conditional instability (Zawadzki et al. 1981), so a reduction in the local contribution to MSE leads to reduced potential for convective precipitation. The Betts and Ball (1998) hypothesis focuses on total local heating of the PBL. Because latent heat flux is not released locally—condensation might occur some distance downwind—it is excluded from consideration. Instead, the hypothesis states that an increase in  $H$ , possibly accompanied by an increase in local radiative heating ( $Q_R$ ), causes a deepening of the PBL due to more vigorous mixing and entrainment at the top of the boundary layer. The combination of deepening and entrainment of dry, low MSE air from the free troposphere leads to reduced MSE density ( $\langle \text{MSE} \rangle$ ) and a higher lifting condensation level (LCL), thus reducing the potential for precipitation.

Comparing 1999 to 2003, the average  $R_{\text{net}}$  for May in the EP was  $16.8 \text{ W m}^{-2}$  less during the drought year of 1999, resulting in a  $15.7 \text{ W m}^{-2}$  decrease in  $Q_t$  (Table 1). Additionally, a slightly cooler ground temperature in 1999 was associated with a  $5.7 \text{ W m}^{-2}$  reduction in the net radiative exchange ( $Q_R$ ) between the surface and the lower atmosphere. Here  $Q_R$  was calculated as a

simple radiative balance,  $Q_R = \varepsilon_a L_{\uparrow} - \varepsilon_s L_{\downarrow}$ , where  $\varepsilon_a$  and  $\varepsilon_s$  are the emissivity of the lower atmosphere and surface, and longwave upwelling ( $L_{\uparrow}$ ) and downwelling ( $L_{\downarrow}$ ) terms are solved based on ground temperature and air temperature near the top of the PBL, respectively (Liou 2002; Zaitchik et al. 2006). The change in  $Q_t$  and  $Q_R$  sum to a reduction of  $22.5 \text{ W m}^{-2}$  in the total local energy transfer between the surface and the lower atmosphere ( $Q_{\text{Total}} = Q_t + Q_R$ ). A forcing of this magnitude is on the order of forcings that have triggered precipitation feedbacks in previous modeling studies (e.g., Schär et al. 1999), though the prevailing aridity of the Middle East may limit the potential for feedback in this region.

In the NZ, in contrast, the 1999 drought was associated with very slight increases in average  $R_{\text{net}}$  ( $1.7 \text{ W m}^{-2}$ ) and  $Q_t$  ( $2.7 \text{ W m}^{-2}$ ) for the month of May. The small change in  $Q_t$  is the result of large offsetting changes in  $H$  ( $+32.4 \text{ W m}^{-2}$  in the drought year) and  $\lambda E$  ( $-29.7 \text{ W m}^{-2}$ ). The minor increase in  $Q_t$  was offset by a decrease in  $Q_R$ , and the difference in  $Q_{\text{Total}}$  between 1999 and 2003 ( $-1.2 \text{ W m}^{-2}$ ) was far too small to trigger any forcing on precipitation via the Eltahir (1998) mechanism. The MM5 results for the NZ are consistent with the Betts and Ball (1998) feedback hypothesis, however, as total local heating ( $H + Q_R$ ) was enhanced by  $28.5 \text{ W m}^{-2}$  in 1999 relative to 2003 and the average depth of the PBL was increased by 87 m. This leads to a deeper, drier PBL, with reduced potential for moist convection.

#### Vegetation reversal

Cloud thickness in MM5 can be estimated by summing the column-integrated fields of all condensed water species (ice, snow, rainwater, and cloud water). Averaged over a month, this “cloudiness” calculation is a proxy for total cloudiness, sensitive to changes in either cloud frequency or cloud thickness. The spatial pattern of the MM5 cloudiness compares relatively well with the MODIS-derived monthly cloud fraction (e.g., Fig. 10).

Comparing simulations  $1999_{V2003}$  and  $1999_{V1999}$  (Fig. 11a), one finds that cloudiness was greater over the northern Zagros and east of the Caspian in the  $1999_{V2003}$  simulation. There was essentially no difference in cloudiness over the EP. In 2003, when the background atmospheric humidity and local evaporation were both higher than in 1999 (Table 2), the presence of nondrought vegetation ( $2003_{V2003} - 2003_{V1999}$ ) results in increased cloudiness over broad areas of the EP, Saudi Arabia, Turkey, the Zagros Plateau, and east of the Caspian Sea (Fig. 11b). For the EP this discrepancy between the 1999 and 2003 vegetation reversal ex-

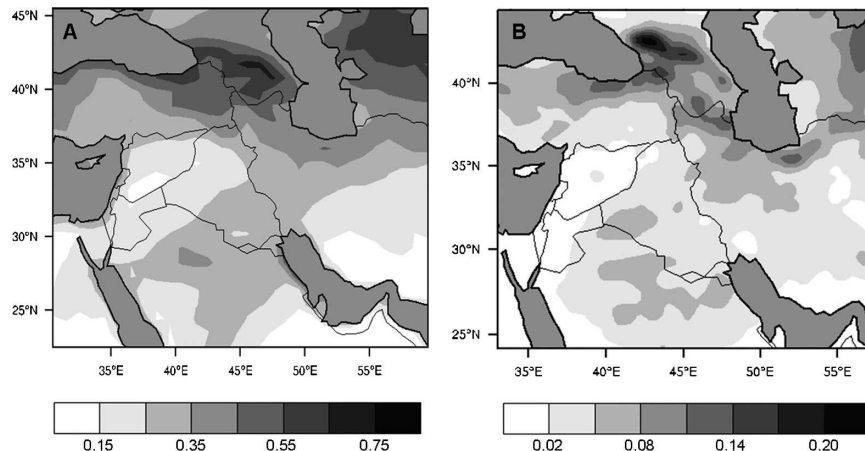


FIG. 10. Cloud cover for May 2003: (a) MODIS monthly average cloud fraction, composited at  $1^\circ$  from MODIS *Terra* and MODIS *Aqua* data; (b) MM5 2003<sub>V2003</sub> column-integrated condensed water content ( $\text{g m}^{-2}$ ), averaged for the month of May and smoothed for comparison with MODIS.

periments is most pronounced in May (Fig. 11c). This supports the suggestion that May is a key month for land–atmosphere forcings on hydrometeorology (section 5). Over the NZ differences in cloudiness are present from April through August in both 1999 and 2003 vegetation reversal experiments, with increased cloudiness observed in simulations with healthy vegetation (1999<sub>V2003</sub> and 2003<sub>V2003</sub>).

The cloudiness result for the EP emphasizes the importance of abiotic factors—primarily soil moisture and mesoscale atmospheric conditions—in determining whether a vegetation forcing will trigger a feedback on the atmosphere. In the wetter, convectively active conditions of 2003 the presence of a healthy vegetation cover had the potential to enhance the production of clouds relative to a simulation with drought vegetation. The dry, convectively stable background conditions of

1999, meanwhile, were relatively resistant to the introduction of an artificially healthy vegetation cover (1999<sub>V2003</sub>), and cloudiness effects were not realized in the EP.

It is difficult to assess the significance of the cloudiness and precipitation results relative to background variability without performing an ensemble of simulations, which was not possible in the presented research. Nonetheless, differences in cloudiness in the vegetation reversal experiments suggest that a vegetation-induced feedback is operating. This evidence of feedback in the MM5 can be attributed to the reversal of vegetation fraction and albedo fields because they were the only variables manipulated in the experiment and because no perturbations were applied to the forcing data.

For the EP, healthy vegetation cover is associated with reduced albedo, enhanced sensible heat flux, and

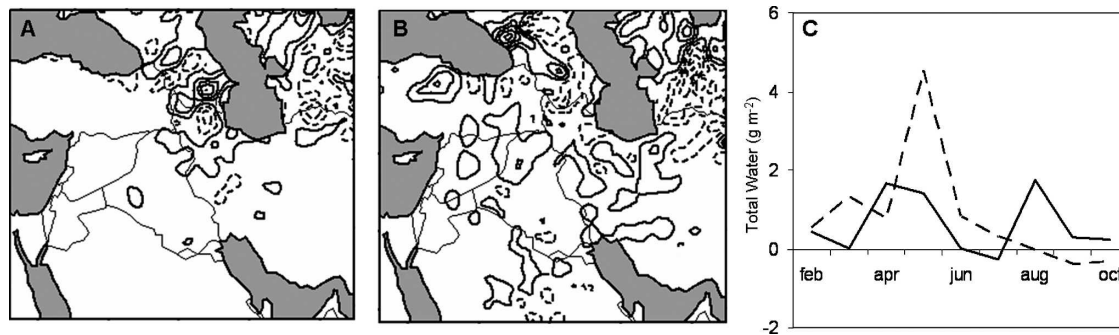


FIG. 11. Column-integrated condensed water content ( $\text{g m}^{-2}$ ): (a) 1999<sub>V1999</sub>–1999<sub>V2003</sub>, (b) 2003<sub>V1999</sub>–2003<sub>V2003</sub>, average values for the month of May. Contour interval is  $8 \text{ g m}^{-2}$ , centered on zero, with negative contours dashed. (c) Time series of monthly averages for 1999<sub>V1999</sub>–1999<sub>V2003</sub> (solid line) and 2003<sub>V1999</sub>–2003<sub>V2003</sub> (dashed line), averaged over the EP.

increased MSE density within the PBL (Table 2). This is consistent with the  $R_{\text{net}}$  drought feedback proposed by Eltahir (1998) and with results of the interannual model comparison described above. In the NZ the vegetation reversal experiments had little impact on surface radiation and total turbulent heat flux. This suggests that vegetation cover on its own does not significantly influence land–atmosphere interactions during drought. Instead, soil moisture may play a more dominant role, through its effects on soil surface properties and its relevance to evapotranspiration. This being the case, differences in NZ cloud cover obtained in vegetation reversal simulations (Figs. 11a and 11b) can be explained in two ways. First, the NZ lies downwind of the EP, so any hydrometeorological forcing in the EP has the potential to impact cloud formation in the NZ. Second, for mountainous areas such as the NZ, the vegetation reversal experiments include some soil moisture effects. This is because portions of the NZ were snow covered through March 2003, while the area was nearly snow-free in March 1999. This snow cover discrepancy affected the SPOT-derived surface albedo, with the result that simulations using the 2003 albedo (i.e., 1999<sub>v2003</sub> and 2003<sub>v2003</sub>) had less early spring evaporation and thus greater residual soil moisture in late spring than the simulations that used the 1999 albedo. Finally, it should be noted that secondary effects of vegetation-induced cloud cover—reduced incident shortwave radiation and enhanced downwelling longwave radiation—were small and offsetting in both regions for both 1999 and 2003 (Table 2).

The distinction between the EP and the NZ is not particularly surprising. In the EP surface moisture is extremely limited in late spring, and evapotranspiration is limited as well. The greatest difference between a drought year and a wet year, then, is that in a wet year the surface albedo is reduced due to greater vegetation cover over bright, dry soils. In the NZ, as indicated in satellite analysis (Fig. 6), interannual variability in albedo is relatively small. Instead, a year of below-average precipitation results in substantial reductions in soil moisture and evapotranspiration. These soil-moisture-induced changes in the surface energy balance form the basis for variability in land–atmosphere interactions.

## 8. Conclusions

In this study it was found that interannual fluctuations in climate lead to considerable variability in vegetation for much of the Middle East. The greatest variability was found in a sensitive transitional climate zone that includes much of the Fertile Crescent and its neigh-

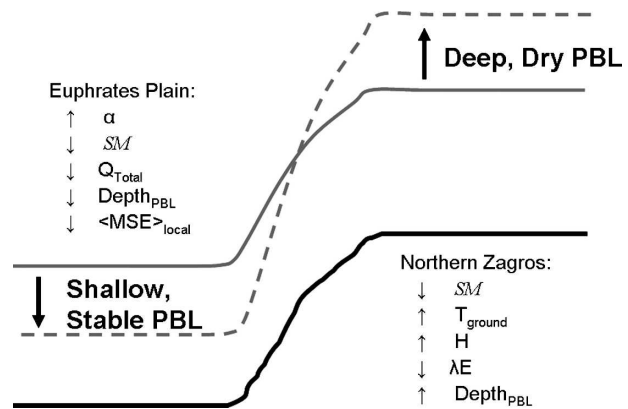


FIG. 12. Surface processes relevant to drought–precipitation forcings in the EP and NZ (schematic): symbols as defined in Table 1. Solid gray line represents the height of the PBL under nondrought conditions and the dashed line represents the height of the PBL during drought. The black line is the land surface.

boring rangelands. In this area vegetation intensity is strongly correlated with surface albedo both during and after the prime growing season. An externally imposed drought, then, leads to reduced vegetation, increased albedo, and the potential for feedbacks associated with changed land surface conditions.

During the drought of 1999, the impact of drought on vegetation, albedo, and soil moisture led to conditions consistent with surface feedbacks on precipitation. In the Euphrates Plain (EP), increased albedo led to reduced local heat flux, producing a shallow, stable planetary boundary layer (PBL) with low conditional instability (Fig. 12). In the neighboring northern Zagros region (NZ), drought led to reduced soil moisture and increased sensible heat flux, causing a deep, dry PBL to develop. This condition is associated with enhanced entrainment of dry air at the top of the PBL and a reduction in conditional instability (Fig. 12). In “vegetation reversal” sensitivity experiments it was found that the drought-related feedback tendency in the EP relied heavily on vegetation status and albedo, while that in the NZ appeared to be more strongly associated with near-surface soil moisture.

The EP is substantially more arid than the NZ. Differences in drought impacts and feedbacks between the two subregions are analogous to differences observed during drought in predominantly arid zones versus more humid regions. In dry areas, vegetation cover is sparse and soils are typically bright. Vegetation drought therefore causes an increase in albedo and a reduced energy environment (Charney et al. 1977; Eltahir 1998). In more humid regions, drought is not necessarily associated with an increase in albedo; senescent vegetation tends to be brighter than live vegetation, and dry

soils are brighter than wet soils (Eltahir 1998), but these effects can be mitigated by resilient vegetation and offset by increased exposure of soils that are relatively dark even when dry (Zaitchik et al. 2006). Under these circumstances feedbacks related to evapotranspiration are expected to dominate, as drought transforms a normally moisture-rich landscape into a moisture-limited environment (e.g., Heck et al. 1999; Sud et al. 2003).

In the Middle East, climate variability is largely a product of external factors, and drought is a common occurrence for both the Euphrates Plain and the more humid—but still drought-prone—Zagros Plateau. In a region that contains steep precipitation gradients and large areas of marginal rain-fed agriculture, any local processes that enhance or mitigate drought are of interest. These processes can include local forcings on air temperature, feedbacks on vapor pressure and cloudiness, and modification of precipitation events. The present study revealed strong evidence for a local influence on temperature, water vapor, and cloudiness during moderate drought, with inconclusive results on precipitation. Further studies of Middle East drought, including analysis of historically extreme or persistent droughts, will further our understanding of land-atmosphere interactions in this environmentally sensitive region.

*Acknowledgments.* This study was carried out with the financial support of NASA Grant NNG05GB36G and with NCAR computer resources made available under NSF Grant ATM-0112354. Preprocessed AVHRR data were provided by Prasad Thenkabail and Praveen Noojipady of the International Water Management Institute (Colombo, Sri Lanka).

#### REFERENCES

- Archer, S., D. S. Schimel, and E. A. Holland, 1995: Mechanisms of shrubland expansion: Land-use, climate or CO<sub>2</sub>. *Climatic Change*, **29**, 91–99.
- Baldocchi, D. D., L. K. Xu, and N. Kiang, 2004: How plant functional-type, weather, seasonal drought, and soil physical properties alter water and energy fluxes of an oak-grass savanna and an annual grassland. *Agric. For. Meteorol.*, **123**, 13–39.
- Betts, A. K., 2004: Understanding hydrometeorology using global models. *Bull. Amer. Meteor. Soc.*, **85**, 1673–1688.
- , and J. H. Ball, 1998: FIFE surface climate and site-average dataset 1987–89. *J. Atmos. Sci.*, **55**, 1091–1108.
- Bright, D. R., and S. L. Mullen, 2002: The sensitivity of the numerical simulation of the Southwest monsoon boundary layer to the choice of PBL turbulence parameterization in MM5. *Wea. Forecasting*, **17**, 99–114.
- Brunsell, N. A., 2006: Characterization of land-surface precipitation feedback regimes with remote sensing. *Remote Sens. Environ.*, **100**, 200–211.
- Charney, J. G., 1975: Dynamics of deserts and drought in Sahel. *Quart. J. Roy. Meteor. Soc.*, **101**, 193–202.
- , W. J. Quirk, S. H. Chow, and J. Kornfield, 1977: Comparative study of effects of albedo change on drought in semi-arid regions. *J. Atmos. Sci.*, **34**, 1366–1385.
- Chen, F., and K. Mitchell, 1999: Using GEWEX/ISLSCP forcing data to simulate global soil moisture fields and hydrological cycle for 1987–1988. *J. Meteor. Soc. Japan*, **77**, 1–16.
- , and J. Dudhia, 2001: Coupling an advanced land surface-hydrology model with the Penn State–NCAR MM5 modeling system. Part II: Preliminary model validation. *Mon. Wea. Rev.*, **129**, 587–604.
- Courel, M. F., R. S. Kandel, and S. I. Rasool, 1984: Surface albedo and the Sahel drought. *Nature*, **307**, 528–531.
- Dall’Omo, G., and A. Karnieli, 2002: Monitoring phenological cycles of desert ecosystems using NDVI and LST data derived from NOAA-AVHRR imagery. *Int. J. Remote Sens.*, **23**, 4055–4071.
- deMenocal, P. B., 2001: Cultural responses to climate change during the Late Holocene. *Science*, **292**, 667–673.
- DePauw, E., 2004: Drought early warning systems for the Near East. *Challenges and Strategies for Dryland Agriculture*, S. C. Rao and J. Ryan, Eds., American Society of Agronomy and Crop Science Society of America, 93–111.
- Dudhia, J., 1993: A nonhydrostatic version of the Penn State–NCAR mesoscale model: Validation tests and simulation of an Atlantic cyclone and cold front. *Mon. Wea. Rev.*, **121**, 1493–1513.
- Eltahir, E. A. B., 1998: A soil moisture rainfall feedback mechanism I. Theory and observations. *Water Resour. Res.*, **34**, 765–776.
- Evans, J. P., and R. Geerken, 2004: Discrimination between climate and human-induced dryland degradation. *J. Arid Environ.*, **57**, 535–554.
- , and R. B. Smith, 2005: Classifying precipitation events in the Fertile Crescent. Preprints, *16th Conf. on Climate Variability and Change*, San Diego, CA, Amer. Meteor. Soc., CD-ROM, 9.4.
- , and R. Geerken, 2006: Classifying rangeland vegetation type and coverage using a Fourier component based similarity measure. *Int. J. Remote Sens.*, **105**, 1–8.
- FAO, 1997: Irrigation in the Near East region in figures. Water Reports 9, U.N. Food and Agriculture Organization, 292 pp. [Available online at <http://www.fao.org/docrep/w4356e/w4356e00.htm>.]
- Geerken, R., and M. Ilaiwi, 2004: Assessment of rangeland degradation and development of a strategy for rehabilitation. *Remote Sens. Environ.*, **90**, 490–504.
- , N. Batikha, D. Celis, and E. Depauw, 2005a: Differentiation of rangeland vegetation and assessment of its status: Field investigations and MODIS and SPOT VEGETATION data analyses. *Int. J. Remote Sens.*, **26**, 4499–4526.
- , B. Zaitchik, and J. P. Evans, 2005b: Classifying rangeland vegetation type and coverage from NDVI time series using Fourier filtered cycle similarity. *Int. J. Remote Sens.*, **26**, 5535–5554.
- Grell, G. A., J. Dudhia, and D. R. Stauffer, 1994: A description of the fifth-generation Penn State/NCAR Mesoscale Model (MM5). NCAR Tech. Note NCAR/TN-398+STR, Boulder, CO, 117 pp.
- Gutman, G., and A. Ignatov, 1998: The derivation of the green vegetation fraction from NOAA/AVHRR data for use in

- numerical weather prediction models. *Int. J. Remote Sens.*, **19**, 1533–1543.
- Heck, P., D. Luthi, and C. Schär, 1999: The influence of vegetation on the summertime evolution of European soil moisture. *Phys. Chem. Earth*, **24B**, 609–614.
- Hole, F., 1994: Environmental instabilities and urban origins. *Chiefdoms and Early States in the Near East: the Organizational Dynamics of Complexity*, Prehistory Press, 121–151.
- Hong, S. Y., and H. L. Pan, 1996: Nonlocal boundary layer vertical diffusion in a medium-range forecast model. *Mon. Wea. Rev.*, **124**, 2322–2339.
- Jacquemin, B., and J. Noilhan, 1990: Sensitivity study and validation of a land surface parameterization using the HAPEX-MOBILHY data set. *Bound.-Layer Meteor.*, **52**, 93–134.
- Kalnay, E., and Coauthors, 1996: The NCEP/NCAR 40-Year Reanalysis Project. *Bull. Amer. Meteor. Soc.*, **77**, 437–471.
- Koster, R. D., and Coauthors, 2004: Regions of strong coupling between soil moisture and precipitation. *Science*, **305**, 1138–1140.
- Kremer, R. G., E. R. Hunt, S. W. Running, and J. C. Coughlan, 1996: Simulating vegetational and hydrologic responses to natural climatic variation and GCM-predicted climate change in a semi-arid ecosystem in Washington, USA. *J. Arid Environ.*, **33**, 23–38.
- Lane, D. R., D. P. Coffin, and W. K. Lauenroth, 1998: Effects of soil texture and precipitation on above-ground net primary productivity and vegetation structure across the central grassland region of the United States. *J. Veg. Sci.*, **9**, 239–250.
- Laval, K., and L. Picon, 1986: Effect of a change of the surface albedo of the Sahel on climate. *J. Atmos. Sci.*, **43**, 2418–2429.
- LeHououerou, H. N., 1996: Climate change, drought and desertification. *J. Arid Environ.*, **34**, 133–185.
- Liang, S. L., C. J. Shuey, A. L. Russ, H. L. Fang, M. Z. Chen, C. L. Walthall, C. S. T. Daughtry, and R. Hunt, 2002: Narrowband to broadband conversions of land surface albedo: II. Validation. *Remote Sens. Environ.*, **84**, 25–41.
- Liou, K. N., 2002: *An Introduction to Atmospheric Radiation*. 2d ed. International Geophysics Series, Vol. 84, Academic Press, 583 pp.
- Los, S. O., 1993: Calibration adjustment of the NOAA AVHRR normalized difference vegetation index without recourse to component channel-1 and channel-2 data. *Int. J. Remote Sens.*, **14**, 1907–1917.
- Mahrt, L., and M. Ek, 1984: The influence of atmospheric stability on potential evaporation. *J. Climate Appl. Meteor.*, **23**, 222–234.
- , and H. L. Pan, 1984: A two-layer model of soil hydrology. *Bound.-Layer Meteor.*, **29**, 1–20.
- Maisongrande, P., B. Duchemin, and G. Dedieu, 2004: VEGETATION/SPOT: An operational mission for the Earth monitoring; presentation of new standard products. *Int. J. Remote Sens.*, **25**, 9–14.
- Matsui, T., V. Lakshmi, and E. E. Small, 2005: The effects of satellite-derived vegetation cover variability on simulated land-atmosphere interactions in the NAMS. *J. Climate*, **18**, 21–40.
- Mlawer, E. J., S. J. Taubman, P. D. Brown, M. J. Iacono, and S. A. Clough, 1997: Radiative transfer for inhomogeneous atmosphere: RRTM, a validated correlated-k model for the long-wave. *J. Geophys. Res.*, **102**, 16 663–16 682.
- Myhre, G., E. J. Highwood, K. P. Shine, and F. Stordal, 1998: New estimates of radiative forcing due to well mixed greenhouse gases. *Geophys. Res. Lett.*, **25**, 2715–2718.
- Nielsen, T. T., and H. K. Adriansen, 2005: Government policies and land degradation in the Middle East. *Land Degradation Development*, **16**, 151–161.
- Pan, H. L., and L. Mahrt, 1987: Interaction between soil hydrology and boundary-layer development. *Bound.-Layer Meteor.*, **38**, 185–202.
- Reisner, J., R. J. Rasmussen, and R. T. Bruintjes, 1998: Explicit forecasting of supercooled liquid water in winter storms using the MM5 mesoscale model. *Quart. J. Roy. Meteor. Soc.*, **124B**, 1071–1107.
- Rodwell, M. J., and B. J. Hoskins, 1996: Monsoons and the dynamics of deserts. *Quart. J. Roy. Meteor. Soc.*, **122**, 1385–1404.
- Schaake, J. C., V. I. Koren, Q. Y. Duan, K. Mitchell, and F. Chen, 1996: A simple water balance model (SWB) for estimating runoff at different spatial and temporal scales. *J. Geophys. Res.*, **101**, 7461–7475.
- Schär, C., D. Luthi, U. Beyerle, and E. Heise, 1999: The soil-precipitation feedback: A process study with a regional climate model. *J. Climate*, **12**, 722–741.
- , P. L. Vidale, D. Luthi, C. Frei, C. Haberli, M. A. Liniger, and C. Appenzeller, 2004: The role of increasing temperature variability in European summer heatwaves. *Nature*, **427**, 332–336.
- Schmidt, H., and A. Karnieli, 2000: Remote sensing of the seasonal variability of vegetation in a semi-arid environment. *J. Arid Environ.*, **45**, 43–59.
- Shukla, J., and Y. Mintz, 1982: Influence of land-surface evapotranspiration on the earth's climate. *Science*, **215**, 1498–1501.
- Small, E. E., and S. A. Kurc, 2003: Tight coupling between soil moisture and the surface radiation budget in semiarid environments: Implications for land-atmosphere interactions. *Water Resour. Res.*, **39**, 1278–1291.
- Sud, Y. C., and M. Fennessy, 1982: A study of the influence of surface albedo on July circulation in semi-arid regions using the GLAS GCM. *J. Climatol.*, **2**, 105–125.
- , and M. J. Fennessy, 1984: Influence of evaporation in semi-arid regions on the July circulation—A numerical study. *J. Climatol.*, **4**, 383–398.
- , and W. E. Smith, 1985: The influence of surface-roughness of deserts on the July circulation (a numerical study). *Bound.-Layer Meteor.*, **33**, 15–49.
- , D. M. Mocko, K. M. Lau, and R. Atlas, 2003: Simulating the midwestern U.S. drought of 1988 with a GCM. *J. Climate*, **16**, 3946–3965.
- Vanacker, V., M. Linderman, F. Lupo, S. Flasse, and E. Lambin, 2005: Impact of short-term rainfall fluctuation on interannual land cover change in sub-Saharan Africa. *Global Ecol. Biogeogr.*, **14**, 123–135.
- Weiss, E., S. E. Marsh, and E. S. Pfirman, 2001: Application of NOAA-AVHRR NDVI time-series data to assess changes in Saudi Arabia's rangelands. *Int. J. Remote Sens.*, **22**, 1005–1027.
- Weiss, H., and R. S. Bradley, 2001: What drives societal collapse? *Science*, **291**, 609–610.
- Weiss, J. L., D. S. Gutzler, J. E. A. Coonrod, and C. N. Dahm, 2004: Long-term vegetation monitoring with NDVI in a diverse semi-arid setting, central New Mexico, USA. *J. Arid Environ.*, **58**, 249–272.
- Xie, P. P., and P. A. Arkin, 1996: Analyses of global monthly precipitation using gauge observations, satellite estimates, and numerical model predictions. *J. Climate*, **9**, 840–858.
- Zaitchik, B. F., J. Evans, and R. B. Smith, 2005: MODIS-derived

- boundary conditions for a mesoscale climate model: Application to irrigated agriculture in the Euphrates basin. *Mon. Wea. Rev.*, **133**, 1727–1743.
- , A. K. Macalady, L. R. Bonneau, and R. B. Smith, 2006: Europe's 2003 heat wave: A satellite view of impacts and land-atmosphere feedbacks. *Int. J. Climatol.*, **26**, 743–769.
- Zawadzki, I., E. Torlaschi, and R. Sauvageau, 1981: The relationship between mesoscale thermodynamic variables and convective precipitation. *J. Atmos. Sci.*, **38**, 1535–1540.
- Zhang, H., A. Henderson-Sellers, A. J. Pitman, J. L. McGregor, C. E. Desborough, and J. J. Katzfey, 2001: Limited-area model sensitivity to the complexity of representation of the land surface energy balance. *J. Climate*, **14**, 3965–3986.
- Zheng, Y. Q., G. Yu, Y. F. Qian, M. Q. Miao, X. M. Zeng, and H. Q. Liu, 2002: Simulations of regional climatic effects of vegetation change in China. *Quart. J. Roy. Meteor. Soc.*, **128**, 2089–2114.
- Ziv, B., H. Saaroni, and P. Alpert, 2004: The factors governing the summer regime of the eastern Mediterranean. *Int. J. Climatol.*, **24**, 1859–1871.